Please note that this is an author-produced PDF of an article accepted for publication following peer review. The definitive publisher-authenticated version is available on the publisher Web site

Journal of Phycology
February 2012, Volume 48, Issue 1, pages 211–221
http://dx.doi.org/ 10.1111/j.1529-8817.2011.01102.x
© 2012 Phycological Society of America

Archimer
http://archimer.ifremer.fr

The definitive version is available at http://onlinelibrary.wiley.com/

Prorocentrum bimaculatum sp. nov. (Dinophyceae, Prorocentrales), a new benthic dinoflagellate species from Kuwait (Arabian Gulf)

Nicolas Chomérat[1,*], Maria Saburova[2], Gwenaël Bilien[1], Faiza Al-Yamani[3]

[1] IFREMER, Station de Concarneau, place de la Croix, 29900 Concarneau, France
[2] Institute of Biology of the Southern Seas, Pr. Nakhimova, 2, 99011, Sevastopol, Ukraine Kuwait Institute for Scientific Research (KISR), Oceanography and Fisheries Research Program, Aquaculture, Fisheries and Marine Environment Dept., P.O. Box 1638, 22017 Salmiya, Kuwait
[3] Kuwait Institute for Scientific Research (KISR), Oceanography and Fisheries Research Program, Aquaculture, Fisheries and Marine Environment Dept., P.O. Box 1638, 22017 Salmiya, Kuwait

*: Corresponding author : Nicolas Chomérat, email address : nicolas.chomerat@ifremer.fr

Abstract :

A new benthic dinoflagellate species, *Prorocentrum bimaculatum* sp. nov., is studied from Kuwait's marine sediments, based on detailed morphological and molecular data. Cells are large, oblong oval in shape. They are 49.9–55.3 µm long and 38.4–43.2 µm wide. The ornamentation of this new species is peculiar, and characterized by smooth valves with large pores (0.32–0.50 µm) scattered on their surface, except in two circular patches of ~15 µm in diameter, devoid of ornamentation and located on both sides of the valve centers. The periflagellar area is widely triangular, located in a moderate excavation of the right valve, and comprises nine platelets. The intercalary band of *P. bimaculatum* is smooth. The molecular phylogenetic position of this new taxon was inferred from SSU and LSU rDNA genes. In both phylogenetic analyses, *P. bimaculatum* branched with high support with *Prorocentrum consutum* and formed a clade sister to the one including *P. lima* and related species such as *P. arenarium*, *P. belizeanum*, *P. hoffmannianum,* and *P. maculosum*. From the phylogenetic study, since most species related to *P. bimaculatum* are known for their toxic effects and production of okadaic acid, this new species can be considered as a potential toxin producer, but this has to be analyzed.

Keywords : Arabian Gulf ; benthic dinoflagellates ; Kuwait ; molecular phylogeny ; morphology, nuclear DNA ; Prorocentrum ; rDNA ; SEM ; taxonomy

Abbreviations: bp, base pairs ; ML, maximum likelihood ; MP, maximum parsimony ; BI, Bayesian inference

Introduction

Members of the genus *Prorocentrum* Ehrenberg constitute a diverse group of marine microalgae with a wide geographical distribution and can contribute a considerable part to benthic dinoflagellate assemblages, especially in sub-tropical and tropical areas (e.g. Faust 1990, Faust 1993a, Faust 1993b, Faust 1994, Faust and Gulledge 2002, Mohammad-Noor et al. 2007b). Many *Prorocentrum* species have been found to produce okadaic acid and can cause diarrhetic shellfish poisoning (DSP) (Faust and Gulledge 2002).

Studies of marine microalgae in Kuwait's marine environment were focused more on the diversity of plankton community than on the composition of benthic species. The diversity of benthic dinoflagellates of Kuwait has been recently reported (Saburova et al. 2009, Al-Yamani and Saburova 2010a, b, Polikarpov et al. 2010) and 58 dinoflagellate taxa were documented during these investigations. Members of the genus *Prorocentrum* were among the most diverse thecate dinoflagellates in this environment. Eight benthic *Prorocentrum* species recorded from Kuwait to date are *P. arenarium* Faust, *P. concavum* Fukuyo, *P. consutum* Chomérat et Nézan, *P. emarginatum* Fukuyo, *P. fukuyoi* Murray et Nagahama, *P. lima* (Ehrenberg) Stein, *P. norrisianum* Faust et Morton, and *P. rhathymum* Loeblich III et al. Among them, five species can be considered as potentially toxic. The cosmopolitan species *P. fukuyoi* is widely distributed throughout Kuwait's intertidal sandflats, and it may be the most abundantly occurring species of all thecate dinoflagellates. Recently described from temperate area (Chomérat et al. 2010), *P. consutum* was found to co-occur with *P. fukuyoi* in sub-tropical Kuwait's intertidal sediments, but at a low abundance.

During the course of our studies on the populations of *P. consutum* from Kuwait's intertidal sediments, we found a *Prorocentrum* species with a very characteristic morphology. It was rather similar to *P. consutum* in size and shape, but it differed in the original pattern of valve pores from not only *P. consutum* but also from all other currently described

65 *Prorocentrum* species. Thus, the aim of this paper is to describe this new species on the basis
66 of light and scanning electron microscopical observations and molecular phylogenetic data.
67
68 **Material and Methods**
69 *Sampling*
70 Kuwait's marine environment is generally shallow with broad flats to the north and a gentle to
71 steep shelf slope along the southern coastline. Height differences of Kuwait's mixed, semi-
72 diurnal tides from low-low water to high-high water are 3.5 to 4 m, and horizontal distances
73 between extreme tidal heights may exceed 8 km in Kuwait Bay. Mean annual temperature of
74 Kuwait's surface water is 23.8ºC, with maximum in July and August, when it ranges from
75 30.5ºC up to 36ºC in shallow waters of Kuwait Bay; temperature minimum coincides with
76 January and February (14ºC, down to 11.9ºC). The mean annual salinity of this area of the
77 Arabian Gulf is 41.6 psu (Al-Yamani et al. 2004).
78 The extended seashore of Kuwait is primarily composed of expansive intertidal flats,
79 which range gradually from mud and sandy mud in the north to medium- or coarse-grained
80 and organically depleted sediments along the southern part of Kuwait's coast. Study of
81 benthic dinoflagellates was undertaken throughout Kuwait's coast from the southern part of
82 Kuwait Bay up to the Saudi border on the south, however, dinoflagellate assemblages with
83 presence of *P. bimaculatum* were recorded only from two sampling sites (Fig. 1) in May-June
84 2010. Site 1 is a small town beach, which is located just outside Kuwait Bay (29º20′26″N,
85 48º05′49″E). Intertidal sediments are composed of rather fine sands with less content of
86 organic matter. Site 2 is located at the southern coast of Kuwait (28º46′58″N, 48º17′40″E).
87 Rather slopping intertidal sandflat is composed of medium- to large-grained and organically
88 depleted sediments.

Intertidal sediments were collected by sampling the upper sediment layer (0-2 cm) from sandy flats, which were exposed at low tide at different intertidal heights using plastic tube corers or flat spoon. The collected samples were transported directly to the laboratory, where dinoflagellates were separated from the sandy sediment by extraction using the frozen seawater method (Uhlig 1964), with a 110 µm mesh size. A part of living material was preliminary observed with a Leica DMIL inverted microscope (Leica, Wetzlar, Germany) at ×35 to ×200 magnifications while a subsample was preserved with 4% neutral Lugol's solution and used for further examinations and molecular analyses.

Light and scanning electron microscopy

Living cells were observed and photographed using a Leica DMLM (Leica, Wetzlar, Germany) microscope fitted with a Leica DFC 320 digital camera. For detailed observations, individual cells fixed in Lugol's solution were isolated from field samples and washed in distilled water using a micropipette under an Olympus IX51 (Olympus, Tokyo, Japan) inverted microscope. Fixed cells were examined in light microscopy with an Olympus BX51 upright microscope equipped with epifluorescence (100W short arc mercury lamp), Nomarski Differential Interference Contrast (DIC) optics and a DP72 digital camera (Olympus). To visualize nuclei, cells were stained for 30 min with 4',6-diamidino-2-phenylindole, dihydrochloride (DAPI, Sigma) fluorochrome (final stain concentration 0.05 µg ml^{-1}) and observed in epifluorescence using an Olympus U–MWU2 fluorescence cube (330–385 nm band pass excitation filter, 400 nm dichromatic beam splitter and 420 nm barrier emission filter).

For scanning electron microscopy (SEM), cells were individually isolated and concentrated in 0.2 ml tubes containing distilled water and a drop of formaldehyde to prevent fungal development. Cells were filtered using polycarbonate membrane filters (Millipore

GTTP Isopore, 0.22 mm pore size), rinsed in deionized water and prepared according to Chomérat and Couté (2008). The examination was performed with a Quanta 200 (FEI, Eindhoven, the Netherlands) scanning electron microscope with an electron acceleration of 5 kV.

Cell dimensions were measured on 8 specimens: one specimen was measured in LM using a calibrated micrometer on the eyepiece, while SEM digital micrographs of seven specimens were processed with ImageJ software (Rasband 1997–2006). SEM photographs were presented on a dark gray background using Adobe Photoshop CS2, v. 9.0.2 (Adobe Systems, San Jose, CA, USA).

DNA amplification and sequencing

After their identification in LM, single cells were isolated from a field sample collected in May 2010 at Site 1 using a micropipette, under an IX51 inverted microscope and transferred onto a glass slide. Each cell was rinsed individually in several drops of double distilled water and then transferred to 0.2 ml PCR tube containing 5 µl of ddH_2O. Then, PCR tubes were stored at –20 °C. For PCR, the samples were thawed and 25 pmol of each primer and 12.5 µl of PCR Master Mix 2X (Promega, Madison, WI, USA) containing the *Taq* DNA polymerase, dNTPs, $MgCl_2$ and reaction buffers, were added in each tube. Two rounds of PCR were realized and 1µl of the dilution (1/100 in ddH_2O) of the PCR product was used as a DNA template for the second round of PCR. Almost the full length of the SSU rDNA (≈ 1800 base pairs) was acquired for isolated cells of *P. bimaculatum* and also *P. consutum* from the same sample.

The polymerase chain reactions for both rounds were performed in a TProfessional Basic thermocycler (Biometra GmbH, Goettingen, Germany) as follows: one initial denaturating step at 94 °C for 2 min, followed by 45 cycles each consisting of 94 °C for 30

sec, 54 °C for 30 sec, and 72 °C for 4 min, and a final elongation of 72 °C for 5 min. The PCR products were purified using the Wizard SV Gel and PCR Clean-up system (Promega) according to the manufacturer's recommendations. The sequencing reaction was realized using the ABI PRISM BigDye Terminator Cycle Sequencing Kit (Applied Biosystems, Carlsbad, CA, USA) and the sequences were determined using an automated 3130 genetic analyser (Applied Biosystems).

Sequences alignment and phylogenetic analyses

The SSU and LSU rDNA sequences obtained were aligned with other putative *Prorocentrum* species and two outgroup (*Scrippsiella* spp.) sequences using MUSCLE algorithm (Edgar 2004) followed by refinement by eye with MEGA software (Tamura et al. 2007), version 4. Genbank accession numbers of all sequences used are available in the supplementary material (Appendix S1).

Evolutionary models were examined for each data set using maximum likelihood (ML), Bayesian inference analysis (BI) and maximum parsimony (MP). The evolutionary model and parameters were selected using jModelTest version 0.1.1 (Posada 2008). According to Akaike information criterion (AIC) and Bayesian information criterion (BIC), a general time reversible (GTR) model with a gamma correction (Γ) for among-site rate variation and invariant sites was chosen for the SSU dataset while a Tamura-Nei (TN93) model with no invariant sites was chosen for the LSU dataset.

Maximum likelihood analyses were performed using PhyML version 3.0 (Guindon and Gascuel 2003), Bayesian analyses were run using Mr Bayes version 3.1.2 (Ronquist and Huelsenbeck 2003) and parsimony analyses with heuristic search were performed using PAUP* version 4.0b for Windows (Swofford 2002). Bootstrap analysis (1000 pseudoreplicates) was used (for ML and MP) to assess the relative robustness of branches

(Felsenstein 1985). Initial Bayesian analyses were run with a GTR model (nst=6) with rates set to invgamma (gamma for LSU dataset). Each analysis was performed using four Markov chains (MCMC), with two millions cycles for each chain. Trees were saved every 100 cycles and the first 2000 trees were discarded. Therefore, a majority-rule consensus tree was created from the remaining 18000 trees in order to examine the posterior probabilities of each clade.

The consensus trees were edited using MEGA 4 software. The two *Scrippsiella* species were used to root the trees. The best ML phylograms are shown with robustness values for each node (ML/BI/MP).

Results

Observations

***Prorocentrum bimaculatum* Chomérat et Saburova sp. nov.** (Figs 2–21)

Descriptio: Organismus unicellularis, photosyntheticus et ovalis. Longitudo: 49.9–55.3 µm; latitudo: 38.4–43.2 µm. Nucleus in medio-posteriori parte locatus et castaneae similis. Valvae laeves cum poris dispersis praeter in duabus circularibus regionibus cum 15 µm diametro utrinque valvae centro locatis. Pori marginales in continuo annulo dispositi in duabus valvis. Pori diameter: 0.32–0.50 µm. Valva recta indentata in apice; valva sinistra cum brevi apicali crista. Regio periflagellaris cum novem parvis lamellis constituta; aliquae parvae lamellae utraequae ex parte tectae et conspicuae solum ex parte. Porus flagellaris ovalis. Accessorius porus ovalis sed in apicale visu dissimulatus. Fascia intercalaris laevis.

Unicellular and photosynthetic organism, oval in shape. Length: 49.9–55.3 µm; width: 38.4–43.2 µm. Nucleus roughly chestnut-shaped, located in medio-posterior part of the cell. Valves smooth with scattered pores, except in two circular areas of 15 µm in diameter, located on both sides of the valves centre. Marginal pores present on both valves. Pore size: 0.32–0.50

μm. Right valve with a moderate excavation at the apex; left valve with a short apical ridge. Periflagellar area composed of nine platelets; some platelets overlapping others and being only partially visible. Flagellar pore oval. Accessory pore oval but hidden in apical view. Intercalary band smooth.

Habitat: marine and benthic

Holotype: Figs 8, 10, 11, SEM stub CEDiT2010H6 stored at the CEDiT (Centre of Excellence for Dinophyte Taxonomy) dinoflagellate type collection, Wilhelmshaven, Germany.

Isotypes: Figs 9, 11, 15. (SEM stub CEDiT2010I7).

Type locality: intertidal sand of the town beach (site 1, 29º20'26"N, 48º05'49"E), Ras Salmiya, Kuwait.

Known distribution: P. bimaculatum was collected from Kuwait's intertidal sediments.

Etymology: From Latin, *bis*, two and *maculatus*, spotted, in reference to the two circular areas without ornamentation, like two round patches on the valves.

The cells are large, 49.9–55.3 μm long (mean 52.5, SD 2.1, n = 8) and 38.4–43.2 μm wide (mean 40.9, SD 1.9, n = 8) in valve view. They are oblong oval, with a length to width ratio ranging from 1.25 to 1.32 (Figs 2–9, 18–19), and flattened (*ca*. 22 μm broad in sagittal suture/intercalary band view). In valve view, the anterior end of the right valve is indented and has a wide V–shaped depression while the left valve forms a slight depression at the apex (Figs 2–3, 6–9, 18–19). The valves are flat to slightly concave in their centre (Fig. 10). The valve surface is smooth with large pores or deep depressions (0.32–0.50 μm in diameter) scattered. A continuous ring of marginal pores runs alongside the periphery of valves (Figs 8–12). The pores form a characteristic pattern on the right and left valves. Two large circular

areas (*ca*. 15 µm in diameter) are devoid of pores, on both sides of the center of each valve (Figs 6–7, 8–9, 11, 16, 18–19). This characteristic has been chosen to name the species, since the valves appear to possess two unornamented patches on their surface. The inside valve surface is smooth, and many pores seem to be grouped by two (Fig. 15), which was not seen in the external view. The intercalary band is smooth (Fig. 12).

The periflagellar area is widely triangular, about 8 µm long and 4.5 µm high, and located in a moderate excavation of the right valve (Figs 8, 11, 13). In apical view, this area is complex and comprises several platelets but some are obscured from view because of the extensions formed by some platelets (Fig. 13). Consequently, only the flagellar pore is partially visible (Fig. 13). Thanks to the observation of the periflagellar area from the inside of a right valve, nine platelets have been identified and named according to Taylor's scheme (Taylor 1980) (Fig. 14). Four platelets "a_1", "d", "f", and "h" border the small apical ridge formed by the left valve (Figs 13, 20), while three other platelets "a_2", "e" and "g" are located on the end of the V-shape (Figs 13–14, 20–21). The flagellar pore is surrounded by the platelets "c", "f", "g" and "e" (Figs 14, 21). It is oval and measures about 1.9 µm in length and 1.2 µm in width (Fig. 14). The accessory pore is totally hidden in apical view because of extensions of the platelets "a_1", 'a_2" and "d", but it is present and clearly visible in the internal view (Fig. 14). It is oval, 1.1 µm long and 0.7 µm wide (Fig. 14). The platelet "b" and the major part of "c", which is the unique platelet separating the flagellar and accessory pores, are hidden in the apical view but seen in the view from the inside (Fig. 14). The platelets visible apically are ornamented with deep depressions (Fig. 13).

Interestingly, on a probably recently-divided cell with a thin theca (Fig. 16), two kinds of pores are observed in the valve center, between the two round patches (Fig. 17). The large pores have the same size than those observed in older cells, and the small pores are 0.14–0.17 µm (Fig. 17).

On living cells, the nucleus is difficult to observe because of the granulated cell content (Figs 2–3). On fixed specimens, it is obscured because of the coloration resulting from the fixation by Lugol's solution (Fig. 4). After DAPI–staining and observation in epifluorescence microscopy, the nucleus appears to be roughly chestnut-shaped, and located posteriorly below the centre of the cell (Fig. 5).

Prorocentrum bimaculatum was found in Kuwait's sediments, in association with other *Prorocentrum* species such as *P. fukuyoi* and *P. consutum* but at a very low abundance.

Sequence analysis and molecular phylogeny

Five identical sequences of SSU rDNA (1789 bp) were acquired from independent cells of *P. bimaculatum* and two identical sequences were obtained for LSU rDNA (974 bp), corresponding to the D1–D3 domains. In addition, two identical sequences of SSU rDNA were acquired from two isolated cells of *P. consutum* to ensure the identification of this species.

The phylogenetic trees inferred from SSU and LSU rDNA showed the existence of two major lineages in the genus *Prorocentrum* identified as clade 1 and clade 2 in the phylograms (Fig. 22). The clade 1 comprised asymmetric species, or those with a variable morphology, including *P. dentatum* Stein, *P. donghaiense* Lu, *P. emarginatum*, *P. fukuyoi*, *P. glenanicum* Chomérat et Nézan, *P. gracile* Schütt, *P. mexicanum* Osorio–Tafall, *P. micans* Ehrenberg, *P. minimum* (Pavillard) Schiller, *P. panamense* Grzebyk et al., *P. pseudopanamense* Chomérat et Nézan, *P. triestinum* Schiller, *P. tsawwassenense* Hoppenrath et Leander and *P. rhathymum* (Fig. 22). The new species *P. bimaculatum* was included in clade 2 which comprised the symmetric species *P. arenarium*, *P. belizeanum* Faust, *P. consutum*, *P. concavum* (including the synonym *P. arabianum*), *P. faustiae* Morton, *P.*

hoffmannianum Faust, *P. levis* Faust et al., *P. lima*, *P. maculosum* Faust and unidentified species "FL3" and "RAV2" (Fig. 22).

The SSU sequence of *P. consutum* from Kuwait grouped with a high statistical support with the sequence from Brittany. The branches of nearly equal lengths indicated that they hardly differ and that they unambiguously belong to the same taxon (Fig. 22A). In phylogenies inferred from the two ribosomal genes, *Prorocentrum bimaculatum* formed a sister-clade to that of *P. consutum.* In the SSU rDNA phylogeny, this position was supported with a high posterior probability (BI) but with weaker values in ML and MP (Fig. 22A) which contrasts with in the LSU phylogeny where it was fully supported (Fig. 22B). Considered together, *P. consutum* and *P. bimaculatum* formed a sister group to the subclade containing *P. lima* and related species*,* including *P. arenarium*, *P. belizeanum* and *P. hoffmannianum*. In the LSU phylogeny, this position was fully supported with bootstraps values of 100 (ML and MP) and a posterior probability of 1.00 (BI), whereas the support was weaker in the SSU phylogeny as only the posterior probability was 1.00 (Fig. 22).

Discussion

In this study, we examined morphological and molecular genetic characters of *P. bimaculatum*, a large and peculiar *Prorocentrum* species found in Kuwait's intertidal sediments. Both morphological and molecular data prove unambiguously that it corresponds to a new taxon. Morphologically, its ornamentation is very peculiar, with two circular areas devoid of pores on each valve. Several species are devoid of ornamentation and thecal pores in the center of valves (Table 1). In contrast, in *P. bimaculatum* some pores are found in the central area between the two circular patches located on both sides of the centre, which differs from all the other *Prorocentrum* species known. Among benthic *Prorocentrum* species, *P. bimaculatum* is a rather large species, exceeding 50 µm in length and thus only slight smaller

than *P. consutum* and *P. belizeanum* (Table 1). This new species is related to *P. consutum*, *P. arenarium* and *P. lima* in having smooth valves bordered by a row of marginal pores (Table 1). From a very recent study, *P. arenarium* has been found to be a synonym of *P. lima* and corresponds to a round morphotype of this species, which means that the outline shape of a taxon is probably not a good taxonomic criterion (Nagahama et al. 2011). The smooth intercalary band observed in *P. bimaculatum* is characteristic of other *Prorocentrum* species, such as *P. belizeanum*, *P. foraminosum* Faust, *P. lima*, and *P. arenarium* (Faust et al. 2008).

In contrast with all these species, the presence of two kinds of pores in *P. bimaculatum* has been noticed on one recently divided cell. Two sizes of thecal pores have been described in several species such as *P. caribbaeum* Faust, *P. emarginatum*, *P. rhathymum*, *P. formosum* Faust, *P. fukuyoi*, *P. elegans* Faust and *P. tsawwassenense*. Most of these species have an asymmetrical morphology and belong to the clade 1 of *Prorocentrum* in phylogenetic studies. Species of the clade 2 which are symmetric and mostly benthic have been reported with only one kind of pores, either large as in *P. lima,* or small as in *P. consutum*. However, it is remarkable that the smaller pores were only observed in a cell with a thin theca, while most of other specimens were found to have large pores only. From this observation, small pores could appear to be temporary during the cell development and they may clog or disappear when the cellulosic theca thickens. The role of these pores is unknown yet.

The periflagellar area of *P. bimaculatum* is characterized by a wide triangular shape, an insertion in a moderate excavation of the right valve and the presence of a short apical ridge of the left valve, which is also found in other species such as *P. belizeanum*, *P. consutum*, *P. hoffmannianum*, *P. sabulosum* Faust, and *P. reticulatum* Faust. However, an apical ridge lacks in *P. arenarium*, *P. lima* and *P. maculosum*. Since the extension of some platelets hide a part of the periflagellar area in SEM, it was necessary to study this small area from the inside of the cell. The use of sectioning and TEM (Mohammad-Noor et al. 2007a)

313 could be used as a useful alternative method to complete these observations but it would be
314 difficult with only a few cells from an environmental sample fixed in Lugol and a culture
315 would be required. The number and arrangement of periflagellar platelets are very similar to
316 that of *P. consutum* with a platelet "a" split in two parts. However, the right valve of *P.*
317 *bimaculatum* is not as deeply excavated as in *P. consutum* and the apical ridge is shorter.
318 Similarly, the periflagellar platelets "a_1" and "d" in *P. consutum* form posteriorly extensions
319 which overlap the pore area and hide the structures located underneath (Chomérat et al. 2010).
320 The molecular genetic phylogenies inferred in this study are congruent with most
321 previous works on the genus *Prorocentrum*, and the split in two lineages has been found in
322 most of previous studies using ribosomal genes (Grzebyk et al. 1998, Saldarriaga et al. 2004,
323 Murray et al. 2007, Faust et al. 2008, Hoppenrath and Leander 2008, Chomérat et al. 2010).
324 The clade 1 groups mostly asymmetric species, or those with a variable morphology, living in
325 plankton or sand-dwelling while the clade 2 includes symmetric species, mostly sand-
326 dwelling (Faust et al. 2008, Hoppenrath and Leander 2008). This result seemed to indicate
327 that the genus *Prorocentrum* is polyphyletic, and in phylogenies inferred from SSU rDNA,
328 Murray et al. (2009) found that it was paraphyletic due to the presence of several intruders.
329 These findings may argue in favour of the reinstatement of *Exuviaella*, as proposed by
330 McLachlan et al. (1997). However, this suggestion has not been followed by taxonomists and,
331 from a morphological point of view, there are presumptions that *Prorocentrum* form a
332 monophyletic group in the evolution of dinoflagellates (Taylor 1980, Fensome et al. 1993).
333 The finding based on molecular analyses, that the group may be polyphyletic and that, by
334 implication, that the peculiar morphology of prorocentroid taxa may be an homoplasious
335 character in dinoflagellates, has appeared puzzling and inexplicable (Murray et al. 2009). The
336 monophyly of the genus has been demonstrated only recently, using multi-genes approaches

337 (Zhang et al. 2007) and including non nuclear genes such as mitochondrial genes like *cox* 1
338 (Murray et al. 2009).

339 Since the sequence of *Prorocentrum consutum* isolated from Kuwait grouped with
340 high support with the sequence from Brittany in our SSU rDNA phylogeny, this species is
341 identified unequivocally. The molecular characterization of this species confirms its
342 morphological identification and first report in another location than the type locality (Al-
343 Yamani and Saburova 2010a). Although *P. consutum* was originally described from a
344 temperate oceanic area (Chomérat et al. 2010), it appears from this study that it is also present
345 in Kuwait where the climate is typically arid and warm (BWh type in Köppen's classification,
346 Peel et al. 2007). Thus, the distribution of this species is not restricted to the temperate area
347 but it is probably widespread. In the phylogenetic analyses, *Prorocentrum bimaculatum*
348 appeared to be more closely related to *P. consutum* than to any other species of the clade 2,
349 which is consistent with the results obtained with morphology. However, its branch length
350 was rather long, indicating several differences between these two species which probably
351 evolved separately for a long period.

352 The capability to synthesize toxins appears to have arisen early in prorocentroid
353 evolution, and, in particular okadaic acid synthesis is present in several species of the clade 2
354 (Murray et al. 2009). At present, no study of any harmful effects by *P. bimaculatum* and *P.*
355 *consutum* (Chomérat et al. 2010) have been undertaken as cultures of these two species are
356 not available yet. However, the production of lipophilic toxins (also known as diarrhetic
357 shellfish poisons, DSP) such as okadaic acid and fast-acting toxins has been demonstrated for
358 all the closely related species in the clade 2, including *P. arenarium*, *P. belizeanum*, *P.*
359 *hoffmannianum*, *P. lima* and *P. maculosum* (Faust and Gulledge 2002). In addition, some
360 other species of the other subclade of clade 2, including *P. concavum*, *P. faustiae* and *P. levis*
361 are also known to produce DSP toxins (Faust and Gulledge 2002, Faust et al. 2008) but no

362 data are available for the unidentified strains (Murray et al. 2009). Consequently, from their
363 phylogenetic relationships *P. bimaculatum* and *P. consutum* could be considered as potential
364 toxin-producers and it would be of an utmost importance to assess their actual capability to
365 synthesize lipophilic toxins in a near future.
366
367 **Acknowledgements**
368 We extend special thanks to Audrey Duval for her help in the search of very rare cells of *P.*
369 *bimaculatum* and Nicolas Gayet for his skilled assistance with SEM. We are grateful to Dr.
370 Alain Couté for translating the description into Latin and to Sylviane Boulben and Karine
371 Chèze for their contribution to the molecular work. We would like to express thanks to Dr.
372 Igor Polikarpov for his valuable support and suggestions.
373
374 **References**
375 Al-Yamani, F. Y. & Saburova, M. 2010a. *Illustrated guide on the flagellates of Kuwait's*
376 *intertidal soft sediments*. Kuwait Institute for Scientific Research, Safat, Kuwait, 197
377 pp.
378 Al-Yamani, F. Y. & Saburova, M. 2010b. First report of ciguatera-associated dinoflagellates
379 in Kuwait's marine environment (abstract). GEOHAB Open Science Meeting on
380 HABs in benthic systems. Honolulu, Hawaii, USA, 21-23 June 2010. p. 23.
381 Al-Yamani, F. Y., Bishop, J., Ramadhan, E., Al-Husaini, M. & Al-Ghadban, A. N. 2004.
382 *Oceanographic atlas of Kuwait's waters*. Kuwait Institute for Scientific Research,
383 Kuwait, 203 pp.
384 Chomérat, N. & Couté, A. 2008. *Protoperidinium bolmonense* sp. nov. (Peridiniales,
385 Dinophyceae), a small dinoflagellate from a brackish hypereutrophic lagoon (South of
386 France). *Phycologia* 47:392-403.

387 Chomérat, N., Sellos, D. Y., Zentz, F. & Nézan, E. 2010. Morphology and molecular
388 phylogeny of *Prorocentrum consutum* sp. nov. (Dinophyceae), a new benthic
389 dinoflagellate from South Brittany (northwestern France). *J. Phycol.* 46:183-94.
390 Edgar, R. C. 2004. MUSCLE: multiple sequence alignment with high accuracy and high
391 throughput. *Nucleic Acids Res.* 32:1792-97.
392 Faust, M. A. 1990. Morphologic details of six benthic species of *Prorocentrum* (Pyrrophyta)
393 from a mangrove island, Twin Cays, Belize, including two new species. *J. Phycol.*
394 26:548-58.
395 Faust, M. A. 1993a. *Prorocentrum belizeanum*, *Prorocentrum elegans*, and *Prorocentrum*
396 *caribbaeum*, three new benthic species (Dinophyceae), from a mangrove island, Twin
397 Cays, Belize. *J. Phycol.* 29:100-07.
398 Faust, M. A. 1993b. Three new benthic species of *Prorocentrum* (Dinophyceae) from Twin
399 Cays, Belize: *P. maculosum* sp. nov., *P. foraminosum* sp. nov. and *P. formosum* sp.
400 nov. *Phycologia* 32:410-18.
401 Faust, M. A. 1994. Three new benthic species of *Prorocentrum* (Dinophyceae) from Carrie
402 Bow Cay, Belize: *P. sabulosum* sp. nov., *P. sculptile* sp. nov. and *P. arenarium* sp.
403 nov. *J. Phycol.* 30:755-63.
404 Faust, M. A. & Gulledge, R. A. 2002. Identifying harmful marine dinoflagellates.
405 *Smithsonian Institution. Contributions from the United States National Herbarium*
406 42:1-144.
407 Faust, M. A., Vandersea, M. W., Kibler, S. R., Tester, P. A. & Litaker, R. W. 2008.
408 *Prorocentrum levis*, a new benthic species (Dinophyceae) from a mangrove island,
409 Twin Cays, Belize. *J. Phycol.* 44:232-40.
410 Felsenstein, J. 1985. Confidence limits on phylogenies: An approach using the bootstrap.
411 *Evolution* 39:783-91.

412 Fensome, R. A., Taylor, F. J. R., Norris, D. R., Sargeant, W. A. S., Wharton, D. I. &
413 Williams, G. L. 1993. A classification of living and fossil dinoflagellates.
414 *Micropaleontol. Spec. Publ.* 7:1-351.
415 Grzebyk, D., Sako, Y. & Berland, B. 1998. Phylogenetic analysis of nine species of
416 *Prorocentrum* (Dinophyceae) inferred from 18S ribosomal DNA sequences,
417 morphological comparisons, and description of *Prorocentrum panamensis*, sp. nov. *J.*
418 *Phycol.* 34:1055-68.
419 Guindon, S. & Gascuel, O. 2003. A simple, fast, and accurate algorithm to estimate large
420 phylogenies by maximum likelihood. *Syst. Biol.* 52:696-704.
421 Hoppenrath, M. & Leander, B. S. 2008. Morphology and molecular phylogeny of a new
422 marine sand-dwelling *Prorocentrum* species, *P. tsawwassenense* (Dinophyceae,
423 Prorocentrales), from British Columbia, Canada. *J. Phycol.* 44:451-66.
424 McLachlan, J.-L., Boalch, G. T. & Jahn, R. 1997. Reinstatement of the genus *Exuviaella*
425 (Dinophyceae, Prorocentrophycidae) and an assessment of *Prorocentrum lima*.
426 *Phycologia* 36:38-46.
427 Mohammad-Noor, N., Moestrup, Ø. & Daugbjerg, N. 2007a. Light, electron microscopy and
428 DNA sequences of the dinoflagellate *Prorocentrum concavum* (syn. *P. arabianum*)
429 with special emphasis on the periflagellar area. *Phycologia* 46:549-64.
430 Mohammad-Noor, N., Daugbjerg, N., Moestrup, Ø. & Anton, A. 2007b. Marine epibenthic
431 dinoflagellates from Malaysia - a study of live cultures and preserved samples based
432 on light and scanning electron microscopy. *Nord. J. Bot.* 24:629-90.
433 Murray, S., Nagahama, Y. & Fukuyo, Y. 2007. Phylogenetic study of benthic, spine-bearing
434 prorocentroids, including *Prorocentrum fukuyoi* sp. nov. *Phycol. Res.* 55:91-102.

435 Murray, S., Ip, C. L. C., Moore, R., Nagahama, Y. & Fukuyo, Y. 2009. Are prorocentroid
436 dinoflagellates monophyletic? A study of 25 species based on nuclear and
437 mitochondrial genes. *Protist* 160:245-64.
438 Nagahama, Y., Murray, S., Tomaru, A. & Fukuyo, Y. 2011. Species boundaries in the toxic
439 dinoflagellate *Prorocentrum lima* (Dinophyceae, Prorocentrales), based on
440 morphological and phylogenetic characters. *J. Phycol.* 47:178-89.
441 Peel, M. C., Finlayson, B. L. & McMahon, T. A. 2007. Updated world map of the Köppen-
442 Geiger climate classification. *Hydrol. Earth Syst. Sci.* 11:1633-44.
443 Polikarpov, I., Saburova, M. & Al-Yamani, F. Y. 2010. Biodiversity of Kuwait's benthic
444 dinoflagellates with emphasis on potentially toxic species (abstract). GEOHAB Open
445 Science Meeting on HABs in benthic systems. Honolulu, Hawaii, USA, 21-23 June
446 2010. p. 30.
447 Posada, D. 2008. jModelTest: Phylogenetic model averaging. *Mol. Biol. Evol.* 25:1253-56.
448 Rasband, W. S. 1997–2006. ImageJ. 1.37c. National Institutes of Health. Bethesda, Maryland.
449 Ronquist, F. & Huelsenbeck, J. P. 2003. MrBayes 3: Bayesian phylogenetic inference under
450 mixed models. *Bioinformatics* 19:1572-74.
451 Saburova, M., Al-Yamani, F. & Polikarpov, I. 2009. Biodiversity of free-living flagellates in
452 Kuwait's intertidal sediments. *In* Krupp, F., Musselman, L.J., Kotb, M.M.A & Weidig,
453 I. (Eds) *Environment, Biodiversity and Conservation in the Middle-East*. *Proceedings*
454 *of the First Middle Eastern Biodiversity Congress. Aqaba, Jordan, 20-23 October*
455 *2008. Biorisk* 3:97-110.
456 Saldarriaga, J. F., Taylor, F. J. R., Cavalier-Smith, T., Menden-Deuer, S. & Keeling, P. J.
457 2004. Molecular data and the evolutionary history of dinoflagellates. *Eur. J. Protistol.*
458 40:85-111.

Swofford, D. L. 2002. PAUP* beta version. Phylogenetic analysis using parsimony (*and other methods). v. 4b4-10. Sinauer Associated. Sunderland, MA.

Tamura, K., Dudley, J., Nei, M. & Kumar, S. 2007. MEGA4: Molecular Evolutionary Genetics Analysis (MEGA) software version 4.0. *Mol. Biol. Evol.* 24:1596-99.

Taylor, F. J. R. 1980. On dinoflagellate evolution. *Biosystems* 13:65-108.

Uhlig, G. 1964. Eine einfache Methode zur Extraktion der vagilen mesopsammalen Mikrofauna. *Helgol. Wiss. Meeresunters.* 11:178-85.

Zhang, H., Bhattacharya, D. & Lin, S. 2007. A three-gene dinoflagellate phylogeny suggests monophyly of Prorocentrales and a basal position for *Amphidinium* and *Heterocapsa*. *J. Mol. Evol.* 65:463-74.

471 **Figure legends**

472 Fig. 1. Map of the Arabian Gulf (top), with inset showing Kuwait's shore, where sampling
473 area was located and map of the Kuwait (lower) showing sampling sites examined; white
474 dots: sampling sites for dinoflagellates surveys (2005–2010), black dots: sampling sites,
475 where *P. bimaculatum* sp. nov. was recorded (May–June 2010), arrow points to type locality
476 of *P. bimaculatum* sp. nov.

477

478 Figs 2–7. Light micrographs of *Prorocentrum bimaculatum* sp. nov. Fig. 2. Living cell in
479 right valve view, with a visible round pusule (pu) near the apex. Fig. 3. The same cell in left
480 valve view. Fig. 4. Cell fixed in Lugol's solution, with a clear area corresponding to the
481 nucleus (n). Fig. 5. DAPI–stained cell observed in epifluorescence, showing the large and
482 chestnut-shaped nucleus. Fig. 6. Right valve of a specimen after dissection (DIC) showing the
483 pore pattern and the two circular patches without ornamentation, the cell content was used for
484 molecular analysis. Fig. 7. Left valve of the same specimen showing the pore pattern and the
485 two circular patches without ornamentation (DIC). Scale bars, = 10 μm

486

487 Figs 8–15. Scanning electron micrographs of *Prorocentrum bimaculatum* sp. nov. Fig. 8.
488 Right valve view of the holotype specimen (SEM stub CEDiT2010H6) showing the pattern of
489 pores and the two circular patches without ornamentation, the row of marginal pores and the
490 excavation of the periflagellar area. Fig. 9. Left valve view of an isotype specimen, showing
491 the row of marginal pores, and the pores pattern with the two circular patches without
492 ornamentation. Fig. 10. Side view of the holotype specimen, showing the sagittal suture of
493 valves. Fig. 11 Anterior view showing the excavation of the triangular periflagellar area. Fig.
494 12. Detail of the thecal surface with pores and smooth intercalary band. Fig. 13. Detail of the
495 periflagellar area of an isotype specimen (SEM stub CEDiT2010I7). Fig. 14. Detail of the

nine periflagellar platelets and the two pores seen from the inside. Fig. 15. Detail of the thecal surface and pores seen from the inside of a valve. Scale bars, 20 μm in Figs 8–10, 10 μm in Fig. 11, 5 μm in Figs 12, 15 and 2 μm in Fig. 14.

Figs 16–17. Scanning electron micrographs of *Prorocentrum bimaculatum* sp. nov. Fig. 16. Left valve view of a young cell with a thin theca, with two kinds of thecal pores, large and small. Fig. 17. Detail of the pores in the central area of the valves with small pores present (arrows). Scale bars, 20 μm in Fig. 15 and 5 μm in Fig. 16.

Figs 18–21. Line drawings of *Prorocentrum bimaculatum* sp. nov. Fig. 18. Right valve view. Fig. 19. Left valve view. Fig. 20. Detail of the periflagellar platelets as seen in apical view. Fig. 21. Interpretation of the arrangement of periflagellar platelets and pores, redrawn from SEM observations. Plain lines indicate actual sutures of the platelets, dotted lines indicate the margin of the extensions of some platelets which partially hide a part of the periflagellar area. Scale bars, 20 μm in Figs 18–19 and 5 μm in Figs 20–21.

Fig. 22. ML phylogenetic trees inferred from SSU rDNA and LSU rDNA. (A) ML tree of *Prorocentrum* species inferred from a SSU rDNA data matrix (34 taxa, 1712 characters). The Likelihood value was found to be loglk = -6760.32692. The tree was rooted using *Scrippsiella* sequences as outgroup. ML analysis was constrained by user-specified settings obtained from jModelTest; model selected: GTR+I+Γ_4. Substitution rate matrix: A↔C = 1.06439, A↔G = 3.73789, A↔T = 1.05823, C↔G = 0.42569, C↔T = 8.57948, against G↔T set to 1.00000 (fixed). Assumed nucleotide frequencies: f(A) = 0.26184, f(C) = 0.20010, f(G) = 0.26347, f(T) = 0.27459. Among-site rate variation: assumed proportion of invariable sites: I = 0.504. Rates at variable site assumed to be gamma distributed with shape parameter: α = 0.709.

Bootstrap values of ML (1000 replicates), posterior probabilities of BI (2,000,000 generations) and bootstrap values of MP (1000 replicates) are shown at nodes in order from left to right, irresolutions noted with '-'. (B) ML tree inferred from a LSU rDNA data matrix (26 taxa, 967 characters). The Likelihood value was found to be loglk = -5884.81206. The tree was rooted using *Scrippsiella* sequences as outgroup. ML analysis was constrained by user-specified settings obtained from jModelTest; model selected: TN93. Assumed nucleotide frequencies: f(A) = 0.22081, f(C) = 0.23378, f(G) = 0.27628, f(T) = 0.26913. Among-site rate variation: assumed proportion of invariable sites: I = 0.149. Rates at variable site assumed to be gamma distributed with shape parameter: α = 0.793. Bootstrap values of ML (1000 replicates), posterior probabilities of BI (2,000,000 generations) and bootstrap values of MP (1000 replicates) are shown at nodes in order from left to right, irresolutions noted with '-'.

Table 1 : Comparison of morphological features of six benthic *Prorocentrum* species related to *P. bimaculatum* sp. nov., and placed in the same subclade of clade 2 in the phylogenetic analyses.

	P. bimaculatum sp. nov. Chomérat et Saburova[a]	*P. consutum* Chomérat et Nézan[b]	*P. arenarium* Faust[c, d, e, f]	*P. lima* (Ehrenberg) Stein[d, e, f]	*P. belizeanum* Faust[d, g, h]	*P. hoffmannianum* Faust[d, i]	*P. maculosum* Faust[j]
Cell shape	Oblong oval	Subcircular to broadly ovoid	Round to slight oval	Ovoid	Round to slight oval	Ovoid	Oval
Cell size [µm]	L: 49.9–55.3, W: 38.4–43.2	L : 57–61, W: 52–55	L: 30–32, W: 30–32[c, d] D: 36–42[e] D: 42–45[f]	L: 31–47, W: 22–40[d] L: 41–43; 31–32[e] L: 38–45, W: 27–38[f]	L: 55–60, W: 50–55	L: 45–55, W: 40–45	L: 40–50, W: 30–40
Theca ornamentation	Smooth with two circular patches devoid of pores	Smooth with a ring of marginal areolae	Smooth	Smooth	Areolate	Areolate	Rugose
Pyrenoid	not observed (?)	Yes, central	Yes, central	Yes, central	Yes, central	Yes, central	Yes, central
Nucleus	Chestnut-shaped, posterior	Kidney-shaped, posterior	?, posterior	Round, posterior	Kidney-shaped, posterior	Large, posterior	Large, posterior
Periflagellar area							
Ridge on left valve	Present, short	Present	Absent	Absent	Present	Present	Absent
No. platelets	9	9	?	8	?	8	8
periflagellar collar	Absent	Present	Absent	Present	Present	Present	Present

Pores							
Marginal pores	Yes	3–4 pores in each marginal areola	Yes (poroids)	Yes	No	No	Yes (poroids)
Valve centre	Two circular areas devoid of pores on both sides of the center	Devoid	Devoid	Devoid	Devoid	Present	Devoid
Pores size [µm]	Two types (temporary?): large: 0.32–0.50 small: 0.14–0.17	0.13–0.17	0.6 µm long, 0.36 µm wide	0.31–0.70	?	?	Mean 0.6
Intercalary band	Smooth	Faintly horizontally striated	Smooth	Smooth	Horizontally striated	Smooth	?

L=length; W=width; D=diameter; ? = no data available; (?) = to be confirmed

References : [a] this study, [b] Chomérat et al. (2010), [c] Faust (1994), [d] Faust and Gulledge (2002), [e] Grzebyk et al. (1998), [f] Mohammad-Noor et al. (2007b), [g] Faust (1993a), [h] Faust et al. (2008), [i] Faust (1990), [j] Faust (1993b).

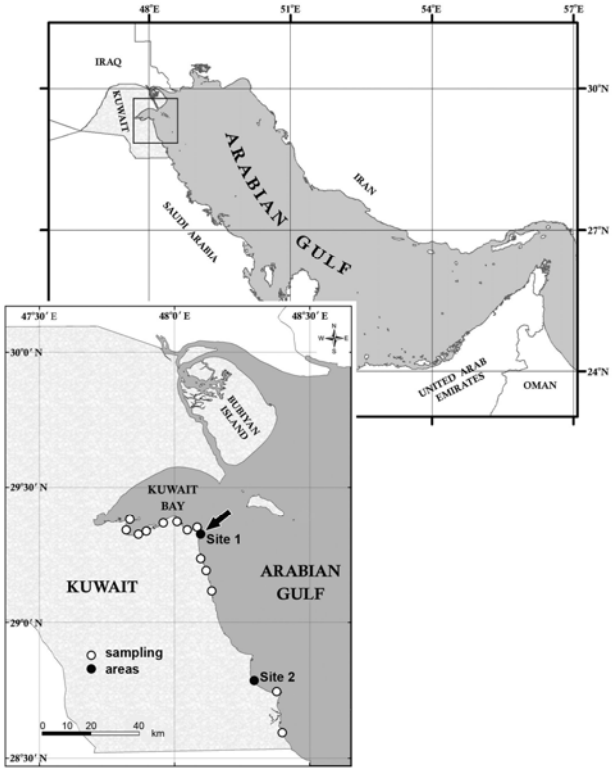
48°E
51°E
54°E
57°E
30°N
27°N
24°N
IRAQ
KUWAIT
SAUDI ARABIA
IRAN
ARABIAN GULF
UNITED ARAB EMIRATES
OMAN
47°30′ E
48°0′ E
48°30′ E
30°0′ N
29°30′ N
29°0′ N
28°30′ N
BUBIYAN ISLAND
KUWAIT BAY
Site 1
Site 2
KUWAIT
ARABIAN GULF
sampling areas
0 10 20 40 km

Fig. 1

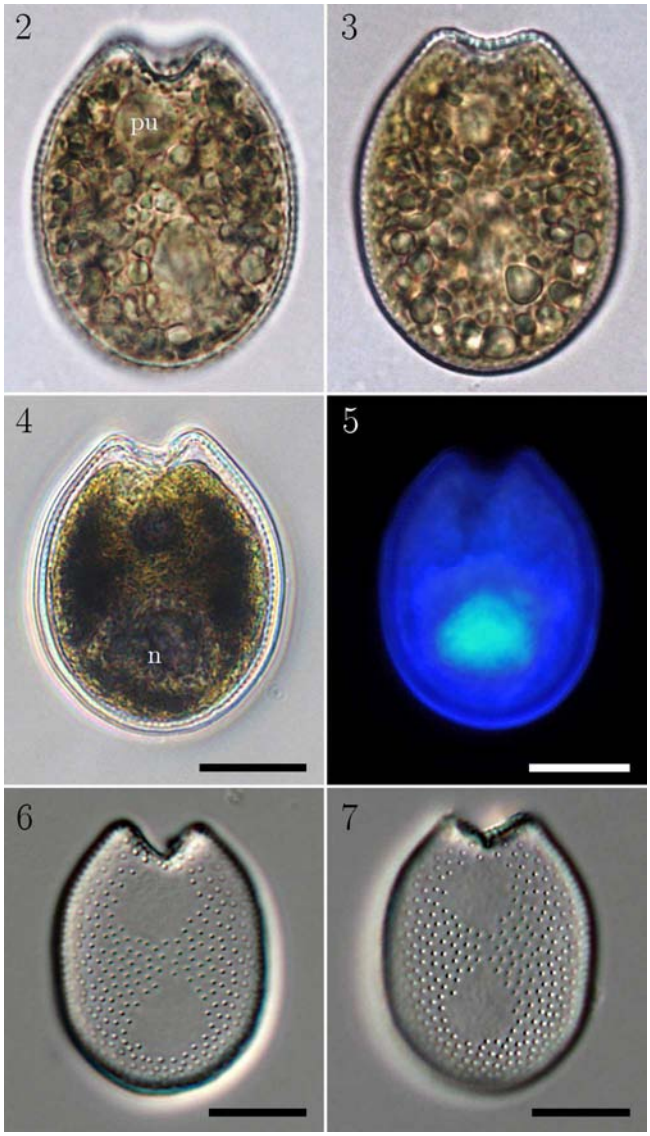
2
pu
3
4
n
5
6
7

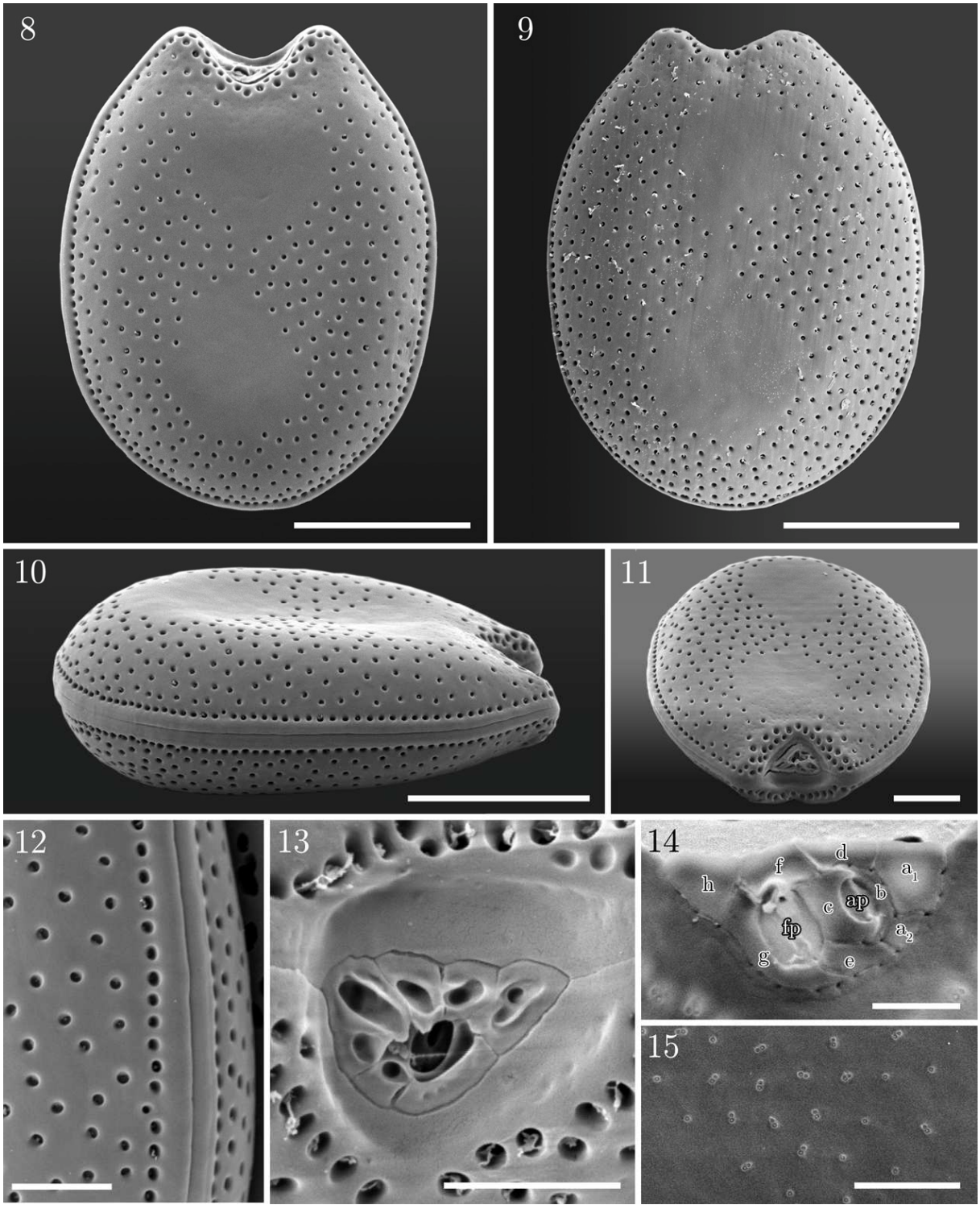
8
9
10
11
12
13
14
d
f
a_1
h
b
ap
c
fp
a_2
g
e
15

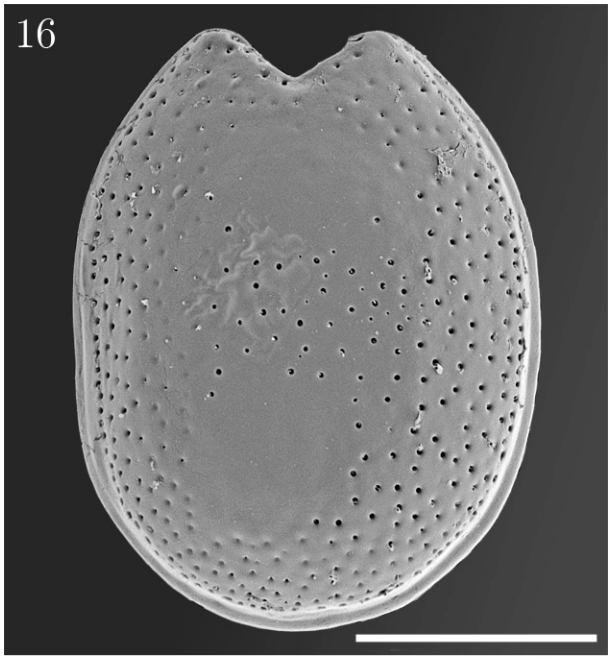
16

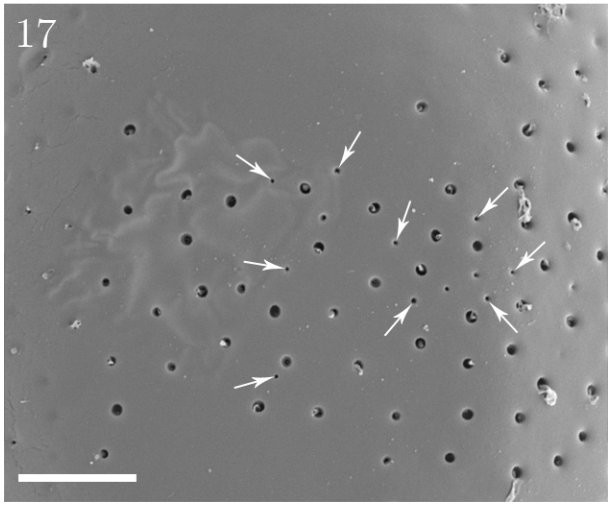
17

18

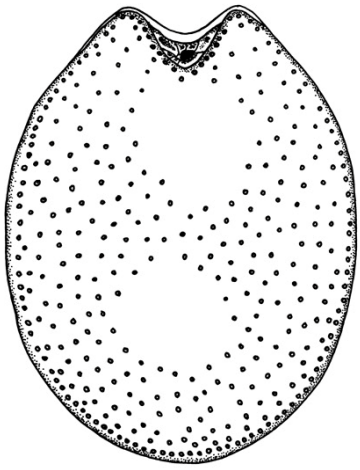

19

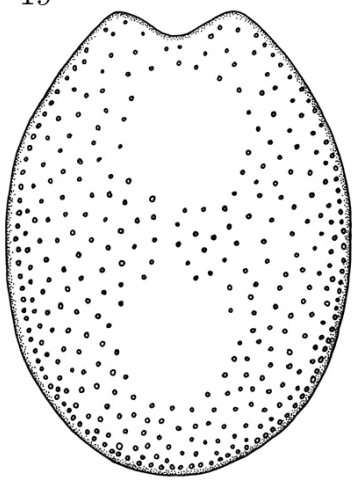

20

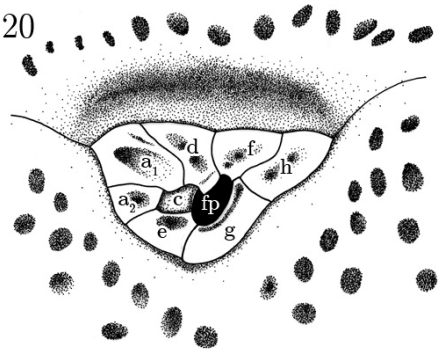

21

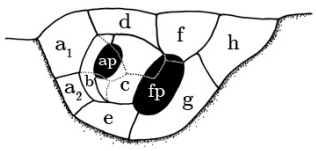

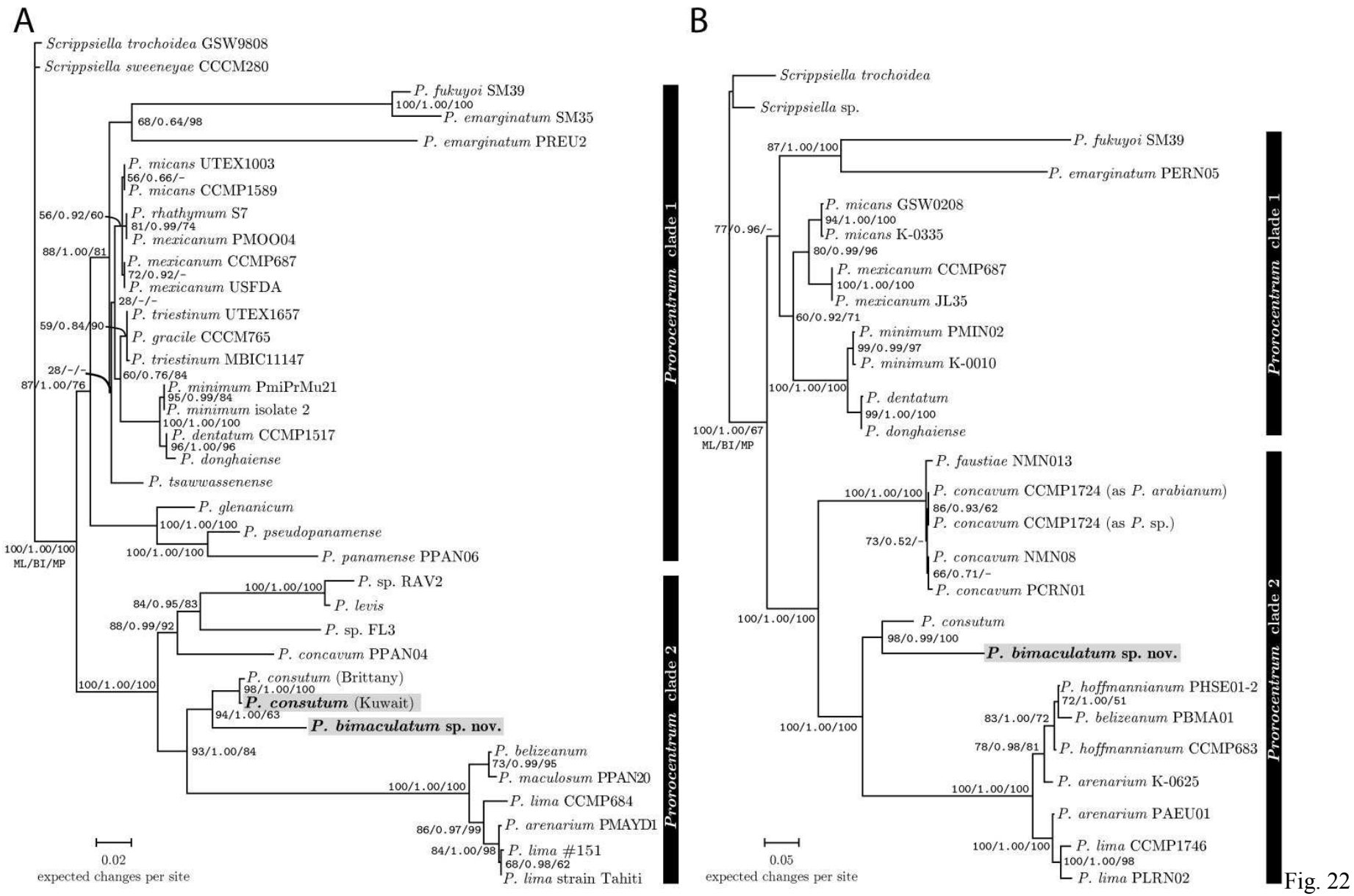
A
Scrippsiella trochoidea GSW9808
Scrippsiella sweeneyae CCCM280
P. fukuyoi SM39
100/1.00/100
P. emarginatum SM35
68/0.64/98
P. emarginatum PREU2
P. micans UTEX1003
56/0.66/-
P. micans CCMP1589
56/0.92/60
P. rhathymum S7
81/0.99/74
P. mexicanum PMOO04
88/1.00/81
P. mexicanum CCMP687
72/0.92/-
P. mexicanum USFDA
28/-/-
P. triestinum UTEX1657
59/0.84/90
P. gracile CCCM765
P. triestinum MBIC11147
28/-/-
60/0.76/84
87/1.00/76
P. minimum PmiPrMu21
95/0.99/84
P. minimum isolate 2
100/1.00/100
P. dentatum CCMP1517
96/1.00/96
P. donghaiense
P. tsawwassenense
P. glenanicum
100/1.00/100
P. pseudopanamense
100/1.00/100
P. panamense PPAN06
100/1.00/100
ML/BI/MP
100/1.00/100
P. sp. RAV2
84/0.95/83
P. levis
88/0.99/92
P. sp. FL3
P. concavum PPAN04
100/1.00/100
P. consutum (Brittany)
98/1.00/100
P. consutum (Kuwait)
94/1.00/63
P. bimaculatum sp. nov.
93/1.00/84
P. belizeanum
73/0.99/95
P. maculosum PPAN20
100/1.00/100
P. lima CCMP684
86/0.97/99
P. arenarium PMAYD1
84/1.00/98
P. lima #151
68/0.98/62
P. lima strain Tahiti
0.02
expected changes per site
Prorocentrum clade 1
Prorocentrum clade 2
B
Scrippsiella trochoidea
Scrippsiella sp.
87/1.00/100
P. fukuyoi SM39
P. emarginatum PERN05
P. micans GSW0208
94/1.00/100
77/0.96/-
P. micans K-0335
80/0.99/96
P. mexicanum CCMP687
100/1.00/100
P. mexicanum JL35
60/0.92/71
P. minimum PMIN02
99/0.99/97
P. minimum K-0010
100/1.00/100
P. dentatum
99/1.00/100
P. donghaiense
100/1.00/67
ML/BI/MP
P. faustiae NMN013
100/1.00/100
P. concavum CCMP1724 (as P. arabianum)
86/0.93/62
P. concavum CCMP1724 (as P. sp.)
73/0.52/-
P. concavum NMN08
66/0.71/-
P. concavum PCRN01
100/1.00/100
P. consutum
98/0.99/100
P. bimaculatum sp. nov.
P. hoffmannianum PHSE01-2
72/1.00/51
83/1.00/72
P. belizeanum PBMA01
78/0.98/81
P. hoffmannianum CCMP683
100/1.00/100
P. arenarium K-0625
P. arenarium PAEU01
100/1.00/100
P. lima CCMP1746
100/1.00/98
P. lima PLRN02
0.05
expected changes per site
Prorocentrum clade 1
Prorocentrum clade 2

Fig. 22